CHARACTERIZATION OF DEFECTS IN ALLOY 152, 52 AND 52M WELDS

S. M. Bruemmer, M. B. Toloczko, M. J. Olszta, R. Seffens and P. Efsing*
Pacific Northwest National Laboratory, P.O. Box 999, Richland, WA 99352
*Ringhals AB, SE-430-22 Varobacka, Sweden

Defect distributions have been documented by optical metallography, scanning electron microscopy and electron backscatter diffraction in alloy 152 and 52 mockups welds, alloy 52 and 52M overlay mockups and an alloy 52M inlay. Primary defects were small isolated grain boundary cracks except for more extensive cracking in the dilution zone of an alloy 52 overlay on 304SS. Detailed characterizations of the dilution zone cracks were performed by analytical transmission electron microscopy identifying grain boundary titanium-nitride precipitation associated with the intergranular separations.

I. INTRODUCTION

Weldments continue to be a primary location of stress-corrosion cracking (SCC) in light-water reactor systems. While problems related to heat-affected-zone (HAZ) sensitization and intergranular (IG) SCC of austenitic stainless alloys in boiling-water reactors (BWRs) have been significantly reduced, SCC has now been observed in HAZs of non-sensitized materials and in dissimilar metal welds where Ni-base alloy weld metals are used. IGSCC in weld metals has been observed in both BWRs and pressurized water reactors (PWRs) with recent examples for PWR pressure vessel penetrations producing the most concern. This has led to the replacement of alloy 600/182/82 welds with higher Cr, more corrosion-resistant replacement materials (alloy 690/152/52/52M). Complicating this issue has been a known susceptibility to cracking during welding [1-7] of these weld metals. There is a critical need for an improved understanding of the weld metal metallurgy and defect formation in Ni-base alloy welds to effectively assess long-term performance.

A series of macroscopic to microscopic examinations were performed on available mockup welds made with alloy 52 or alloy 152 plus selected overlay and inlay mockups with alloy 52 or 52M. The intent was to expand our understanding of weld metal structures in simulated LWR service components with a focus on as-welded defects. Microstructural features, defect distributions, defect characteristics and weld residual strains were examined by optical metallography, scanning electron microscopy (SEM) and electron backscatter diffraction (EBSD). Selected higher resolution characterizations were conducted using transmission electron microscopy (TEM). Industry-supplied mock-up welds were characterized including alloy 52 and 152 weldments, alloy 52M overlay and inlay welds, and an alloy 52 overlay.

II. WELDMENTS

II.A. Alloy 52 and 152 Weld Mockups

The alloy 52 and 152 weld mockups were fabricated by MHI for the Kewaunee reactor and were obtained from the EPRI NDE Center. The mockups were U-groove welds joining two plates of 304SS as shown in Figure 1. Alloy 152 butter (heat 307380) was placed on the U-groove surface for both mockups by shielded metal arc welding (SMAW). For the alloy 152 weld mockup, the alloy 152 fill (heat 307380) was also applied using SMAW while for the alloy 52 weld mockup, the alloy 52 fill (heat NX2686JK) was applied using gas tungsten arc welding (GTAW). Welding parameters for the fill materials were substantially different with the alloy 152 SMAW having a deposition speed of 4-25 cm/min with a current of 95-145 A and the alloy 52 GTAW having a deposition speed of 4-10 cm/min with a current of 150-300 A.

One prominent feature in these mockup welds is the presence of a crack starting at the 304SS butt joint at the bottom of the U-groove and extending up into the weld. It appears that the 304SS plate on either side of the butt joint acted as an anchor for the weld resulting in a stress rise across the slit that drove crack formation and extension up into the fill weld. As will be shown in the next section, the extent of the cracking around this stress riser was much greater in the MHI 52 weld mockup.

II.B. Alloy 52M/182 Overlay, Alloy 52M/82 Inlay and Alloy 52/304SS Overlay Mockups

The alloy 52M/182 overlay mockup was obtained from Ringhals and is shown in Figure 2(a). It was fabricated by robotically welding a 10-mm-thick alloy 52M layer onto alloy 690 plate and then by manually welding alloy 182 onto the alloy 52M layer. The alloy 52M layer was applied by GTAW with a weld speed of 7.5 cm/min at a current of 130 A while the alloy 182 was applied by SMAW with a weld speed of 7-12 cm/min at a current of 95-125 A.

The inlay mockup was obtained from Westinghouse and is from a full-scale inlay repair demonstration by Ringhals on a ring of A533 steel pipe. A boat was carved out of the inner surface of the ring, and as shown in Figure 2(b), alloy 82 fill was robotically welded onto the pipe section. This was followed by the robotic application of the alloy 52M inlay. Complicating this overlay was the manual application of an alloy 152 top layer by Westinghouse to allow fabrication of compact tension specimens for stress-corrosion testing with an orientation allowing cracks to be grown from the alloy 82 into the alloy 52M.

The final overlay mockup material was obtained from Ringhals as an example of weld cracking in the dilution zone created between alloy 52 weld metal and 304SS. Small metallographic samples of an alloy 52 overlay on a 304SS housing were received for high-resolution crack characterizations.

III. METALLOGRAPHIC DEFECT CHARACTERIZATIONS

The general approach for all weld defect characterization activities was to polish and etch the available slices from the mockups to reveal the weld and base metal microstructures. Based on the weld structure, a cut plan was devised, and the large slices were cut down into a series of smaller pieces that were mounted and polished to a 1-μm finish with colloidal silica. Weld defects and cracks were identified by optical metallography, while SEM and EBSD characterizations were performed on selected regions.

III.A. Alloy 152 Weld Mockup

Three slices of the alloy 152 weldment were examined for weld defects. An example of one of the slices is shown in Figure 3(a). The small green boxes indicate areas that showed features that contained possible weld defects. Most indications were small pits probably resulting from inclusion or precipitate pullout during polishing. Only a single short intergranular (IG) crack was found near the main crack that extended from the butt joint at the bottom of the U-groove weld. The largest crack was found in the alloy 152 butter near the 304SS interface and possibly in a region of altered composition. Only a few cracks and no other weld defects were detected in the alloy 152 weld.

III.B. Alloy 52 Weld Mockup

The macroscopic crack in the alloy 52 fill weld extends into the alloy 52 fill weld as shown in Figure 3(b). Many IG cracks were identified in the alloy 52 weld metal around this macroscopic crack with typical examples shown in Figure 4. These cracks were oriented roughly parallel to the large main crack and vary in length from ~10 to 800 μm. The remainder of the alloy 52 weld metal was free of any cracks or other weld defects.

SEM and EBSD examinations focused on several regions having extensive distributions of IG cracks. The EBSD IPF-Z image in Figure 5 enables a better visual image of the individual weld metal grains and highlights areas of plastic deformation. The typical large, elongated grains can be seen along with a collection of very fine grains along certain grain boundaries. The fine grains associated with the IG cracks suggest that local recrystallization may play some role in the cracking process. High strains depicted by large changes in crystal orientation within a grain are found at many of the high-angle grain boundaries and within the interior of many of the grains. Other regions examined also showed a mixture of large, elongated grains and local regions of very fine, recrystallized grains. As expected, high strains were found associated with cracks and grain boundaries in this entire region. Compositional mapping by energy dispersive x-ray spectroscopy (EDS) in the SEM revealed moderate solidification segregation (e.g., Nb and Mn), but no differences were detected at grain boundaries or associated with the IG cracks. It is important to note that the resolution of SEM-EDS analysis is limited and fine-scale segregation or precipitation will not be detected. Additional examinations by ATEM are planned to better define the grain boundary characteristics that may be involved in the cracking process. Examples of this approach to investigate crack tips and grain boundaries on the nanoscale are given later in Section IV.

III.C. Alloy 52M/182 Overlay Mockup

An overview of the front face slice from the alloy 52M overlay mockup piece is shown in Figure 6. Alloy 690 plate is at the bottom of the piece with the alloy 52M welded onto the 690 and the alloy 182 welded onto the alloy 52M. A comparatively large number of cracks were identified with many clustered in three local regions of the overlay. Examples of the cracks are presented in Figure 7 along with the etched microstructure showing them to be IG. Similar clusters of weld cracks were also found at matching locations on the back face slice of the alloy 52M overlay mockup suggesting some characteristic difference in the weld material or welding practice in these regions. The majority of the weld cracks appeared to be randomly placed in each of the three local regions, but there were many small weld cracks associated with the first alloy 52M weld pass near the alloy 690 interface (cut area 8 in Figure 6). Several cracks were also found in the alloy 182 weld metal. SEM, EBSD and ATEM exams are planned to better define the grain boundary characteristics that may be involved in the cracking process in the alloy 52M overlay.

III.D. Alloy 52M/82 Inlay Mockup

Three slices of the alloy 52M inlay were characterized and an overview of one cross-section is shown in Figure 8. The small green boxes again identify sections that were

examined in detail. Several short and long cracks were observed in the alloy 52M inlay with two examples of longer weld cracks shown in Figure 9. The weld cracks were clustered in one region slightly to the right of center of the slice (cut area 6, boxes D and E in Figure 8). Only a few small cracks were found in the alloy 52M weld metal for other two slices with more identified near the alloy 152 interface region and in the alloy 82 weld metal. Only the cracks in the alloy 52M inlay were examined in some detail to document their size and IG morphology.

To document the crack characteristics in more detail, selected SEM and EBSD exams were performed on cracks in alloy 52M weld metal. An EBSD pattern quality image and an inverse pole figure image about the Z axis (IPF-Z) of a short IG crack are shown in Figure 10. Color variation in the EBSD IPF-Z image represents variation in crystal orientation with red representing the 001 zone axis pointing out of the image, green representing the 011 zone axis pointing out of the image, and blue representing the 111 zone axis pointing out of the image (as shown in the inset legend). The IPF shows several interesting features. The step change in color above and below the crack indicates that the crack lies on a high-angle grain boundary, and it can be seen that the crack propagated along a straight section of grain boundary and ended in the adjoining grain matrix at an inclusion particle as the boundary turned ~90 degrees. Color variation in the grain below the crack indicates significant plastic deformation, especially just below the crack where the color changes from green to yellow and then to red. SEM-EDS maps revealed solidification segregation (e.g., Nb and Mn) in the grain matrices, but no strong compositional variation associated with the grain boundaries or IG cracks.

III.E. Summary of Observed Weld Cracks

The only significant defects identified within the as-deposited alloy 152, 52 or 52M weld metals were IG cracks. No evidence for other weld defects was found during the metallographic examinations of the cross-section samples. While the general appearance of the weld cracks was similar among the four mockups, their number densities, lengths and distributions were quite different. Most crack lengths were typically less than ~200 μm with openings varying from <1 to ~10 μm. It should be noted that only a few cross-section slices were evaluated for each material and serial polishing was not performed to assess the 3D aspect of the observed cracks.

The fewest cracks were identified in the alloy 152 weld metal. A sharp macroscopic crack in the alloy 152 was present at the base of the U-groove weld extending from the initial 304SS plate and butter butt joint. Even for this higher-stress location, only isolated IG cracks were found (quite different than for the alloy 52 weld). Only two other weld cracks were confirmed in the alloy 152 cross-sections, one near the top of the weld and the other near the butter interface off to one side of the weld. The total areal number density of cracks in the alloy 152 mockup was less than 0.05 cm^{-2} with a maximum crack length of ~300 μm.

The alloy 52 U-groove weld revealed a substantial amount of weld cracks clustered around the main crack that ran up into the fill weld from the 304SS plate and butter butt joint. This main crack was much more open than seen in the alloy 152 weld indicating much higher local stresses. The areal number density versus crack length for the alloy 52 slices is shown in Figure 11(a). Although the weld cracks were isolated to the region around the large macroscopic weld crack that grew from the base of the U-groove, the entire area of the slice was used to calculate the areal number density. If the area used in the calculation is confined to the region near the main crack, the number density would increase by a factor of ~10. Although this local high-stress region showed a high density of cracks, it is important to note that no other cracks were found in the alloy 52 weld.

The greatest number of weld cracks was found in the alloy 52M overlay. They were clustered in three local regions on both cross-section slices examined. The areal number density versus size distribution for cracks in the alloy 52M overlay is shown in Figure 11(b). The peak in the weld crack length is ~25 μm with the number density falling off rapidly as the weld crack length increases. The majority of the cracks were randomly located in the three regions, however there was an indication that the first alloy 52M weld pass near the alloy 690 interface had a slightly larger number of cracks.

The final mockup examined for weld crack distributions was the alloy 52M inlay, and the areal density of cracks is shown in Figure 11(c). As with the overlay, the crack length peaks at ~25 μm with the distribution tailing off to a very low density of longer cracks. The density of cracks in the inlay is much less than for the overlay particularly in the 25 μm length range. Most of the cracks were found near the final alloy 52M weld pass in this rather thick inlay. Only isolated cracks were identified in the alloy 52M near the alloy 82 interface. The weld cracks in the alloy 52M were typically less than 100 μm in length, but there was a single observation of a ~500 μm crack in the final weld pass. There is insufficient information to determine whether these cracks formed during the application of the alloy 52M inlay mockup by Ringhals or whether it formed during the application of the final alloy 152 overlay by Westinghouse.

Overall, low densities of small IG cracks were found in the alloy 152, 52 and 52M weld metals. The alloy 52M overlay exhibited the most cracking and was localized to selected regions. Even in this case, the IG cracks were well separated in the cross-sections. As noted previously,

higher resolution characterizations are being performed to determine possible microstructural reasons for the formation of weld cracks in as-deposited alloy 52 or 52M weld metals.

IV. ATEM CHARACTERIZATIONS OF WELD CRACKS IN AN ALLOY 52/304SS OVERLAY

Selected high-resolution characterizations have been performed on an overlay mockup containing weld cracks supplied by Ringhals. The alloy 52 overlay on a stainless steel housing represents a standard welding procedure and the appearance of cracks in the mixing (dilution) zone was unexpected. This zone has also been referred to as a sacrifical layer with a non-optimized composition between the 304SS base metal and the alloy 52 weld metal. An example of the overlay appearance is presented in Figure 12 and one of the two metallographic samples supplied by Ringhals shown in Figure 13. Light oxalic etching of the metallographic samples clearly delineated the alloy 52 weld metal and the 304SS based metal. Weld cracks were found in the brighter re-melted regions adjacent to the 304SS, i.e., regions A, B, X and Y.

General compositions in these regions were obtained by SEM-EDS and found to be at an intermediate composition between the alloy 52 and the 304SS. These estimated compositions are listed in Table 1 and reveal Fe at levels of 25-36 wt% and Ni levels of 35-46 wt% for regions with hot cracks. Base concentrations for Fe and Ni in alloy 52 were ~10 and ~60 wt%, while Fe and Ni levels in the 304SS were ~68 and ~8 wt%. Therefore, extensive melting and interdiffusion has occurred during the first overlay passes on the stainless steel resulting in a dilution zone over several mm. An additional example of this dilution zone in relation to the presence of hot cracks is shown by the SEM-EDS map for Fe in Figure 14. Several passes are indicated by the change in relative Fe concentration with hot cracks located primarily in the region where the Fe and Ni are nearly equal in composition (30-35 wt%). The microstructural changes in this dilution zone are also dramatic as illustrated in the EBSD image in Figure 15. SEM and EBSD images reveal the transition from the fine, equiaxed grains in the 304SS base metal into the large, elongated grains in the melted dilution zone.

TABLE I. Measured Compositions by SEM-EDS from Regions in Weld Overlay Dilution Zone

Analysis Region	Ni, wt%	Fe, wt%	Cr, wt%	Ti, wt%
A	45.6	25.0	27.5	0.42
B	36.5	35.6	26.9	0.34
C	50.5	19.3	29.2	0.46
D	53.5	15.8	29.1	0.51
X	35.5	35.3	27.4	0.30
Y	44.8	25.2	28.8	0.47

The next key step in the characterization of the Ringhals overlay samples employed ATEM for the high-resolution examination of grain boundaries and cracks. TEM cross-section samples containing cracks were prepared from the VY3 and VY4 materials by dimple grinding and ion milling. Before cutting and at various times during subsequent preparation, the cracks were protected from contamination during the preparation process by vacuum impregnating the cracks with Gatan G-1 thermosetting resin. Small pieces containing the selected crack regions were cut out and glued to 3-mm-diameter Mo support washers with the targeted features at the centers. After trimming away excess material, the disk samples were flat-ground and finish polished to <100 μm total thickness from the non-washered side. The samples were then dimple-ground from the washer side to ~15 μm thickness, and briefly ion milled with 5 keV argon ions at ±6° incidence to improve the surface finish for SEM examinations. Ion milling was later continued to develop thin areas suitable for TEM analysis, with final milling performed at reduced energy and beam incidence (2 keV, ±4°) to minimize superficial ion-beam damage. Repeated cycles of ion milling and examination were used to progressively thin the cracks and crack-tip areas for examination. Prior to final thinning for TEM, the finish-polished samples were examined by SEM using backscattered electron (BSE) imaging to observe the cracks and metallurgical grain structures. An example of this documentation is presented in Figure 16 from the VY3 material. These observations were used to guide final thinning of regions containing selected cracks and crack tips.

A large number of crack tips have been examined and analyzed from the dilution zone regions of the overlay samples VY3 and VY4. All cracks were IG following high-energy grain boundaries containing second-phase precipitates. The most consistent feature at grain boundaries leading the weld cracks was the presence of TiN either as an elongated thin phase or film on the boundary or discreet fine particles. The TEM image and elemental maps in Figure 17 highlight the thin elongated Ti-rich phase along a grain boundary leading an IG weld crack. In some locations, the <50 nm thick TiN platelet reaches more than a μm in length. Cr-rich $M_{23}C_6$ carbides are also common at grain boundaries, but tend to be well spaced and nearly spherical. More importantly, the elongated Ti phase was also found coating one wall of open cracks. This is presented in Figure 18, which is a higher resolution examination of the same crack tip in Figure 17. The Ti compositional map reveals the presence of the 20-nm thick phase on the lower crack wall suggesting that the crack formed at the Ti precipitate interface during cooling. The crack appears to have stopped at a small $M_{23}C_6$ particle that separates the elongated Ti platelets. Electron diffraction shows that the

Ti-rich phase has a MC crystal structure and electron energy loss spectroscopy has clearly indicated that it is a Ti nitride (TiN) and not TiC.

Several crack-tip regions have been documented and most show a nearly continuous layer of TiN associated with the weld cracks. The exception was for one crack tip where TiN was found as a high density of fine particles and not as an elongated thin phase. $M_{23}C_6$ particles were not always present near the tips, but were seen along boundaries within several μm of this location. The carbides were more spherical in shape, well spaced along the boundary length and separated by lengths of TiN.

Various TEM examinations were also performed in regions of the weld outside of the dilution zone and away from the regions with weld cracks. While grain boundary microstructures varied, the most significant difference appeared to be the distribution of TiN particles. Isolated particles were occasionally identified on boundaries with a moderate density of $M_{23}C_6$ carbides, but a nearly continuous IG phase was only found in the dilution zone region containing the weld cracks. Based on these results, grain boundary TiN is believed to play an important role in the cracking observed for this alloy 52 overlay on 304SS. More work is needed to understand TiN precipitation in the dilution zone and the specific processes leading to IG cracking.

V. CONCLUSIONS

A primary goal of these initial examinations was to assess defects in prototypic, industry-produced, alloy 52 and 152 mockup welds. As described in Section III, weld metals were characterized in three different structures: (1) alloy 52 and 152 U-groove weld mockups; (2) an alloy 52 M overlay and (3) an alloy 52M inlay. The only significant defects identified were IG cracks and, for the most part, these were small and few in number. While the typical crack size in all the welds was 100 μm or less, in three of the weld mockups, several 500 μm long cracks were observed. This length is insufficient for a single crack to span even a thin inlay or overlay, but a clustering of interconnected cracks may potentially provide a path through a thicker weld metal layer. This seems unlikely based on the current limited results, however more detailed studies of crack size and 3D distributions are needed to better assess the probability that such interconnected cracks could exist.

Another important issue is that these pre-existing IG cracks may act as sites for stress-corrosion crack growth during LWR service. The location and length of a weld crack in the inlay or overlay would obviously have a strong affect on the local stress intensities. An IG weld crack that intersects the surface would be subject to a higher stress, and its morphology may promote initiation of an IG stress-corrosion crack. If clusters of weld cracks are present, they may act to facilitate propagation even though typical growth rates in these high-Cr weld metals are extremely slow.

Another potential issue is whether the microstructure and microchemistry in the regions of weld cracks is inherently more susceptible to stress corrosion. This could result from local deformation-induced structures, segregation-induced microchemistries or second-phase precipitation particularly associated with grain boundaries where pre-existing cracks are present. High-resolution ATEM examinations of weld cracks in the alloy 52 overlay demonstrate that unexpected microstructures and microchemistries may be involved in the cracking process. In this case, the formation of layered TiN at grain boundaries was localized to the dilution zone between the alloy 52 and stainless steel. Similar research is needed to better understand the formation of weld cracks in the weld metals and their potential effects on subsequent LWR component reliability in service. Further characterization of these (and other) weld mockups are planned to improve understanding of the root cause of the cracking. This intent will be to evaluate the influence of weld cracks and any associated microstructural-microchemical variations on stress corrosion crack initiation and propagation.

ACKNOWLEDGMENTS

Support from the U.S. Nuclear Regulatory Commission is recognized under Contract DE-AC06-76RLO 1830 along with helpful interactions with A. A. Csontos, C. Moyer and D. S. Dunn. In addition, support for this research was obtained from Ringhals AB. Special thanks are given to Al McIlree and Greg Fredrick for supplying the alloy 52 and 152 weld mockups. Technical assistance of Dan Edwards, Alan Schemer-Kohrn and Clyde Chamberlin are acknowledged. Pacific Northwest National Laboratory is operated for the U.S. Department of Energy by Battelle Memorial Institute.

REFERENCES

1. B. Hood and W. Lin, "Weldability Testing of Inconel Filler Materials," *Proc. 7th Int. Symp. Environmental Degradation of Materials in Nuclear Power Systems – Water Reactors,* NACE International, Breckenridge, CO, 1995, p. 69.
2. W. Wu and C. Tsai, "Hot Cracking Susceptibility of Fillers 52 and 82 in Alloy 690," *Metall. Trans.,* 30A (1999) 417.
3. M. Collins and J. Lippold, "An Investigation of Ductility Dip Cracking in Nickel-Based Filler Materials – Part I," Welding J., 82-10 (2003) 288s.

4. M. Collins, A. J. Ramirez and J. Lippold, "An Investigation of Ductility Dip Cracking in Nickel-Based Filler Materials – Part II," Welding J., 82-12 (2003) 348s.
5. M. Collins, A. J. Ramirez and J. Lippold, "An Investigation of Ductility Dip Cracking in Nickel-Based Filler Materials – Part III," Welding J., 83-2 (2004) 39s.
6. H. Hanninen, A. Toivonen, A. Brederholm, T. Saukkonen, U. Ehrnsten and P. Aaltonen, "Environment-Assisted Cracking and Hot Cracking of Ni-Base Alloy Dissimilar Metal Welds," *Proc. 13th Inter. Conference on Env. Deg. of Materials in Nuclear Power Systems*, Canadian Nuclear Society, Whistler, B.C., 2007.
7. G. A. Young, T. E. Capabianco, M. A. Penik, B. W. Morris and J. J. McGee, "The Mehanism of Ductility Dip Cracking in Nickel-Chromium Alloys," *Welding J.,* 87-2 (2008) 31s.

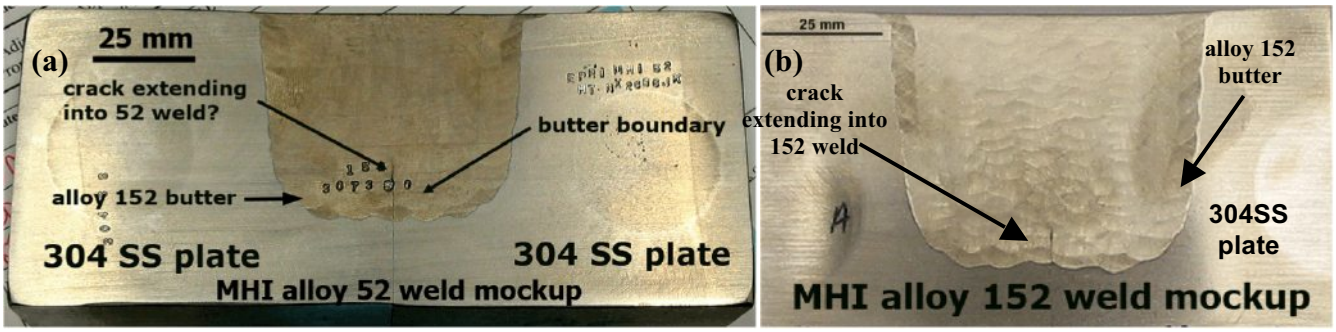

Figure 1. Optical images of alloy 52 (a) and alloy 152 (b) weld mockups showing U-groove welds in cross-section. Both welds were made to 304SS plate using an alloy 152 butter layer.

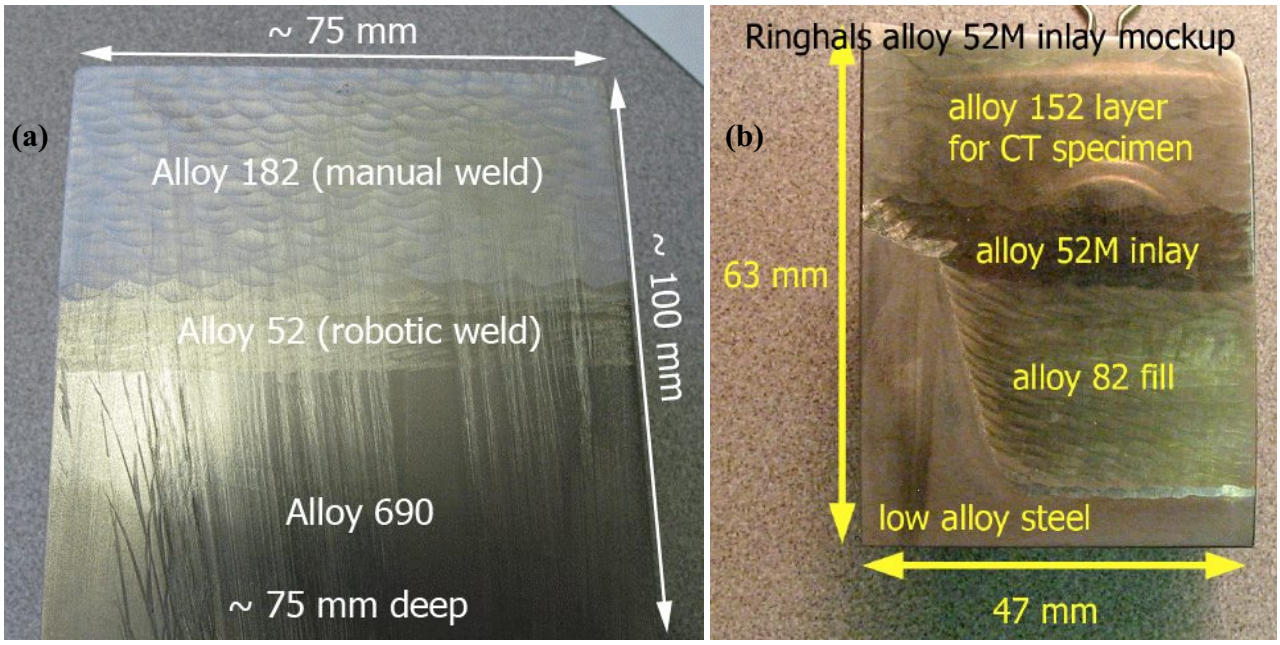

Figure 2. Overview of the Ringhals alloy 52M overlay and inlay mockups: (a) overlay where alloy 52M was robotically welded to an alloy 690 plate followed by alloy 182 manually welded onto the alloy 52M. The alloy 52M layer is 10-mm thick. (b) full-scale, service mockup with alloy 82 fill followed by an alloy 52M inlay. Alloy 152 was welded onto the alloy 52M by Westinghouse to allow fabrication of CT specimens from the inlay region.

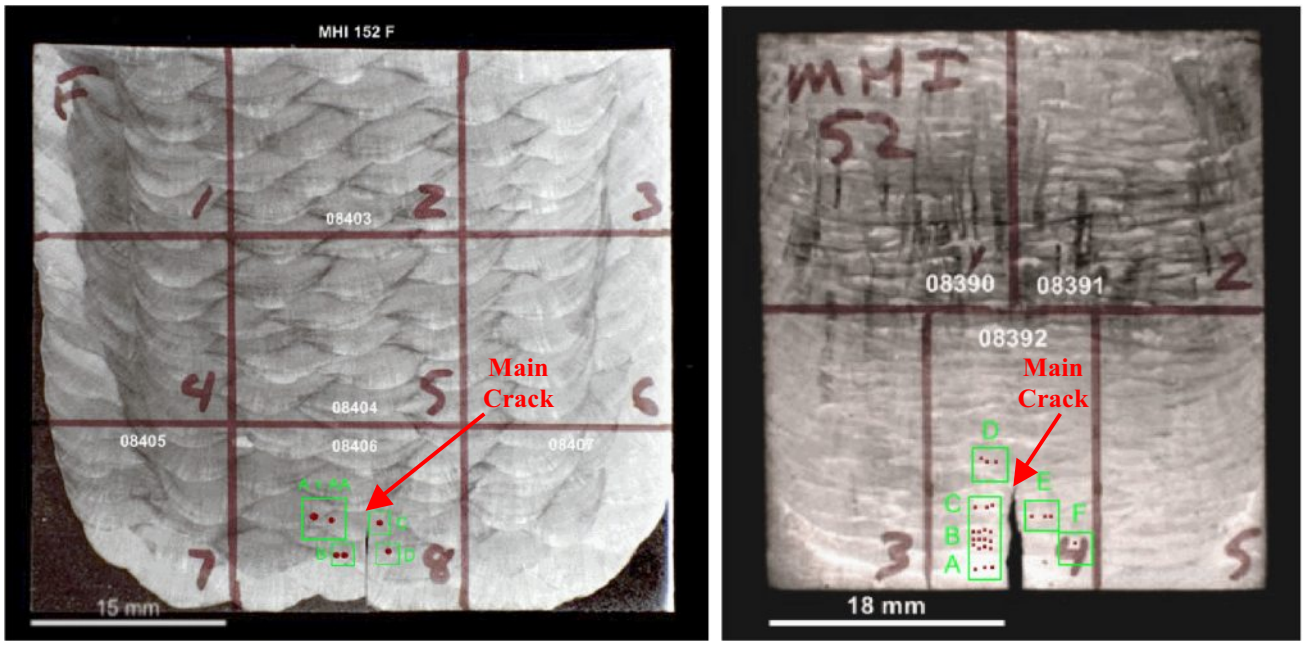

Figure 3. Optical images of the alloy 152 (a) and alloy 52 (b) weld slices with areas showing weld defects highlighted by the green boxes. Cracks in alloy 52 were only found near the main crack location.

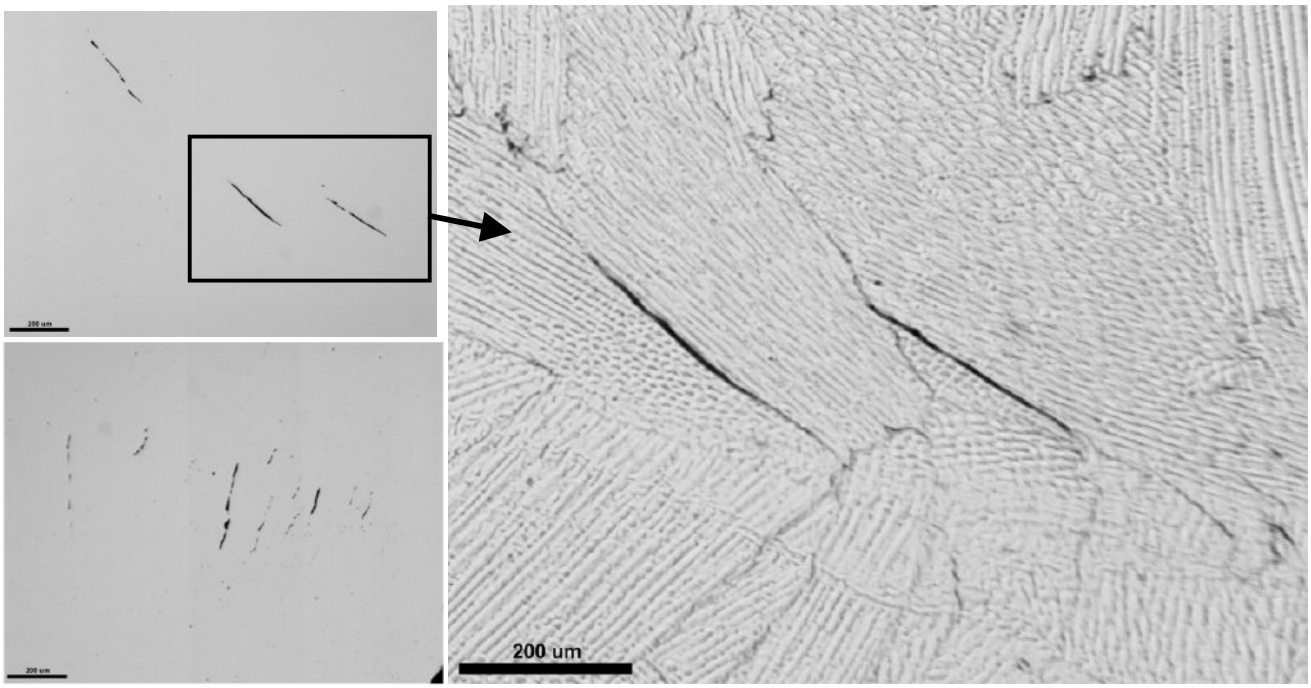

Figure 4. Examples of cracks in alloy 52 weld metal are shown in (a) and (b) near main crack above plate butt joint, while typical IG morphology is illustrated in (c).

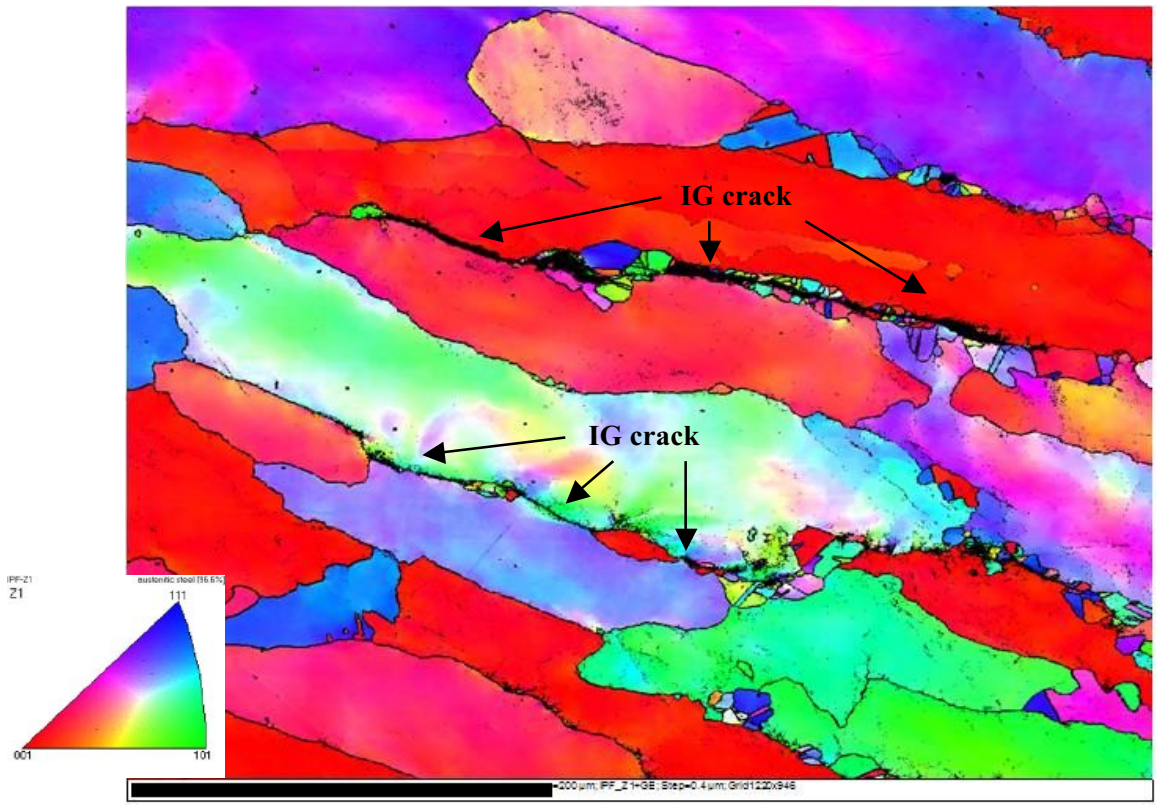

Figure 5. EBSD IPF-Z illustrating the differences in grain orientations in the vicinity of the alloy 52 weld cracks.

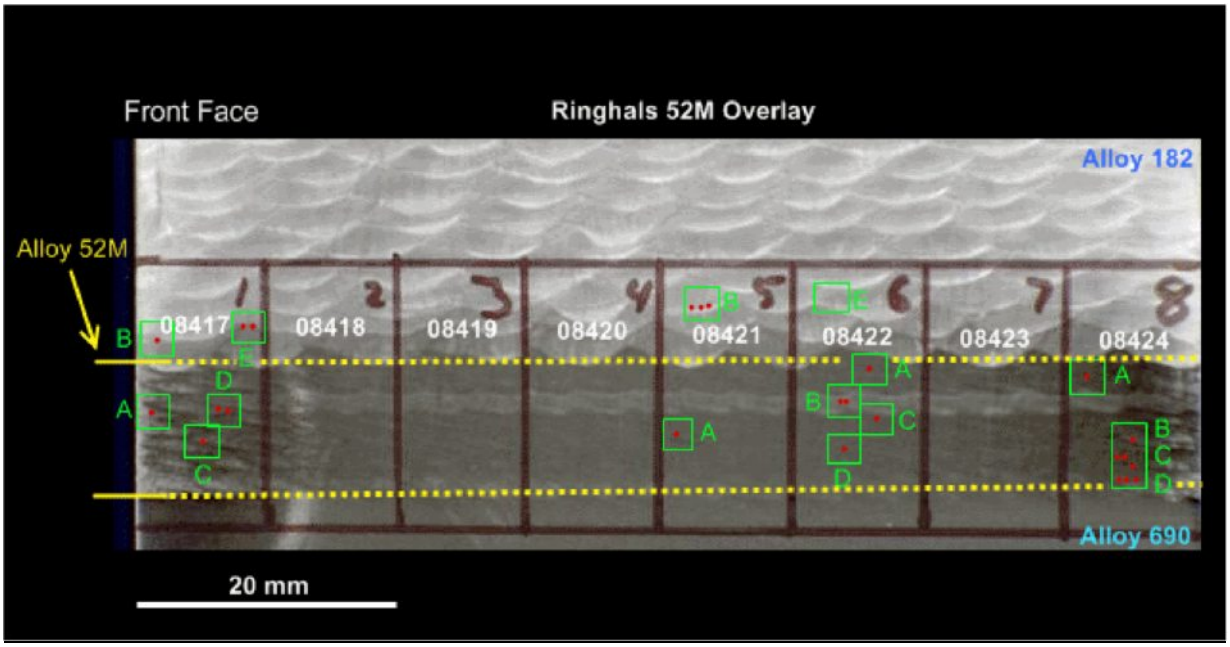

Figure 6. Optical micrograph of the alloy 52M – alloy 182 overlay showing the alloy 690, alloy 52M and alloy 182 layers along with selected regions where cracks were identified in slice A (front face). Cracks were clustered in three local regions within cut diagram areas 1, 6 and 8.

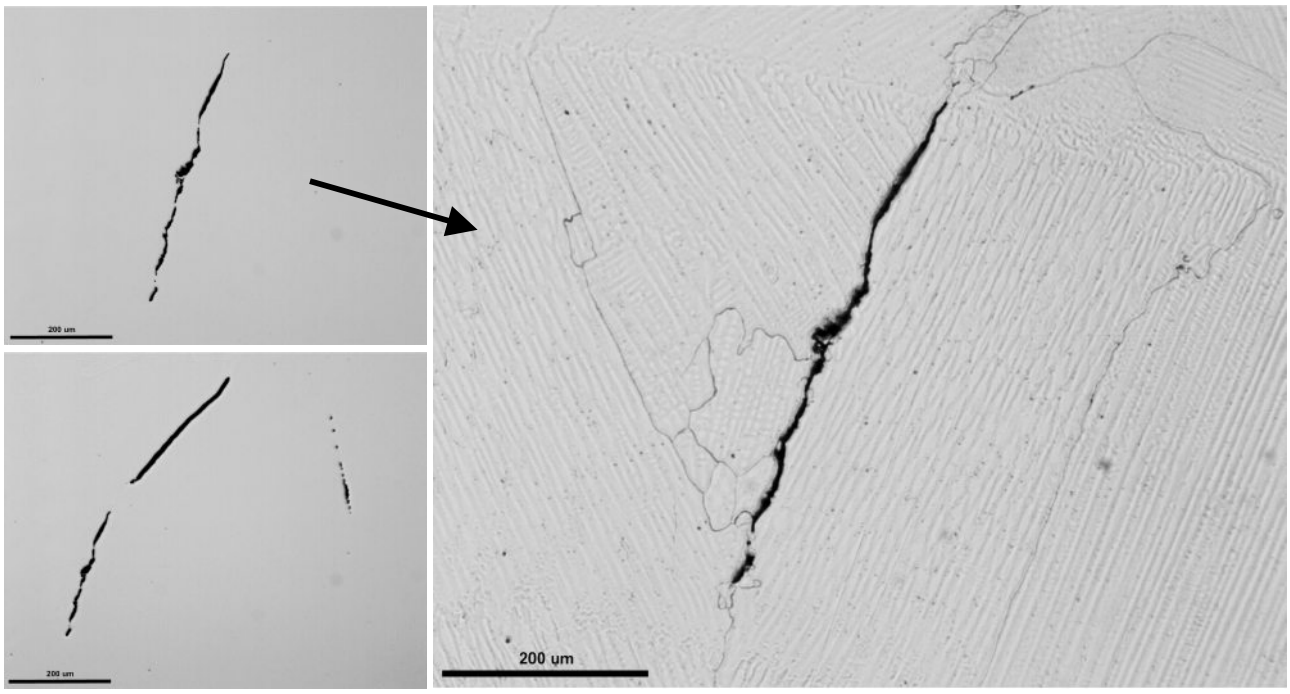

Figure 7. Etched weld microstructure is shown to illustrate the typical morphology of the cracks in the alloy 52M overlay.

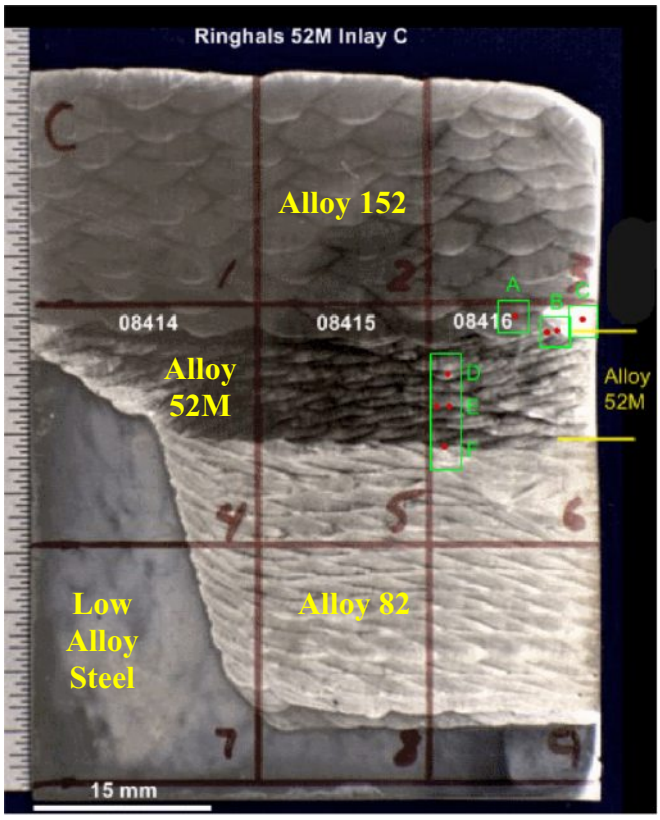

Figure 8. Overview image of the inlay mockup slice C showing regions where weld defects were found and analyzed. Only a few cracks were observed in alloy 52M weld metal.

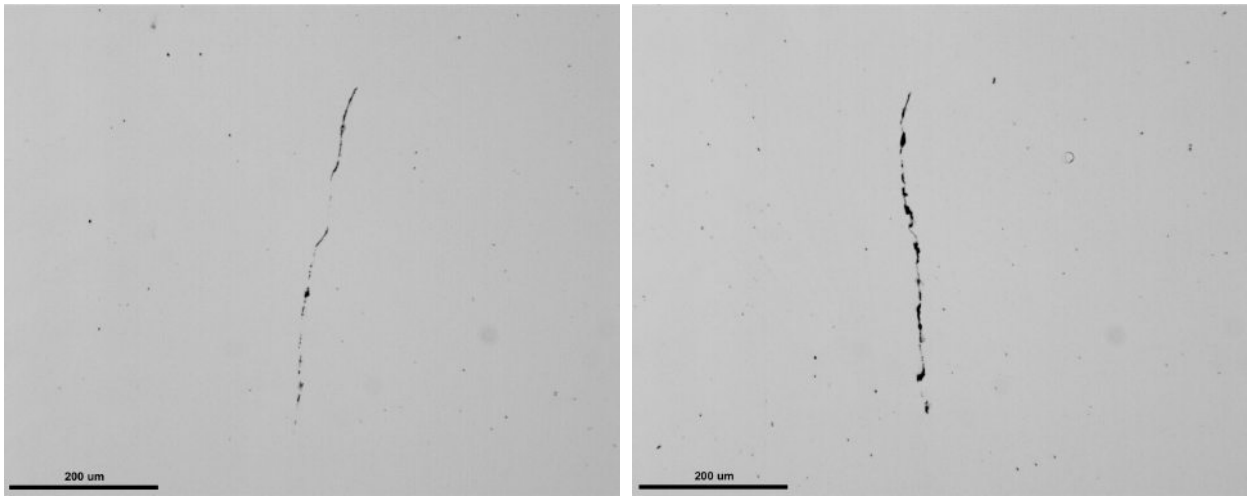

Figure 9. Two examples of isolated IG weld cracks found in the alloy 52M inlay.

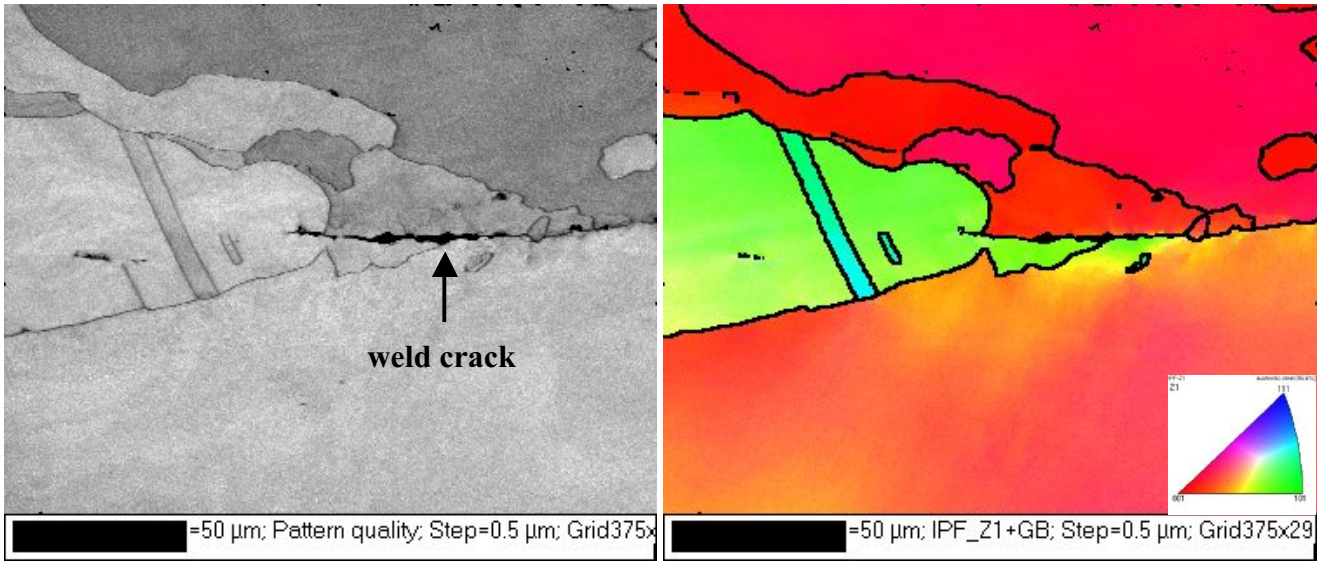

Figure 10. EBSD pattern quality and IPF-Z images of a weld crack in the alloy 52M inlay showing the weld metal microstructure and crack morphology. The main crack runs along a high-angle grain boundary and the minor transgranular cracking appears to be associated with inclusions.

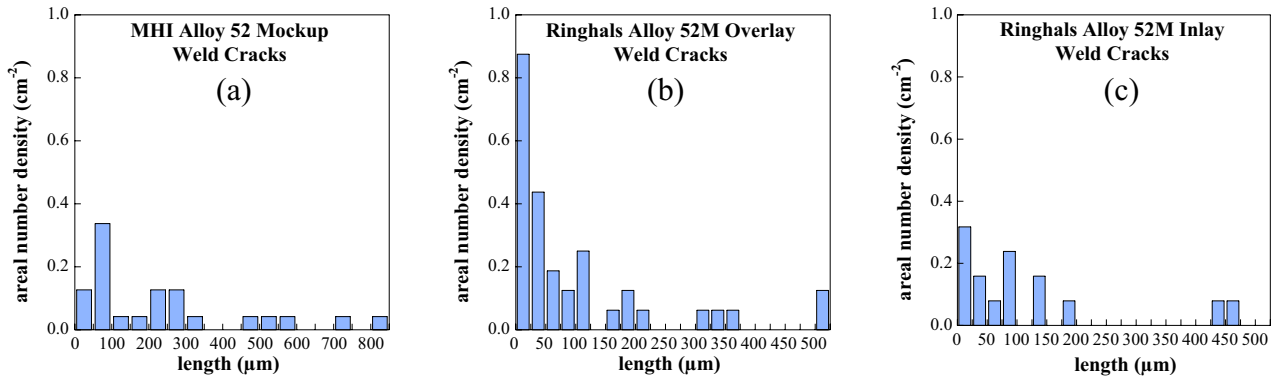

Figure 11. Areal number density versus crack length for the weld cracks observed in the alloy 52 (a), alloy 52M overlay (b) and alloy 52M inlay (c) mockups.

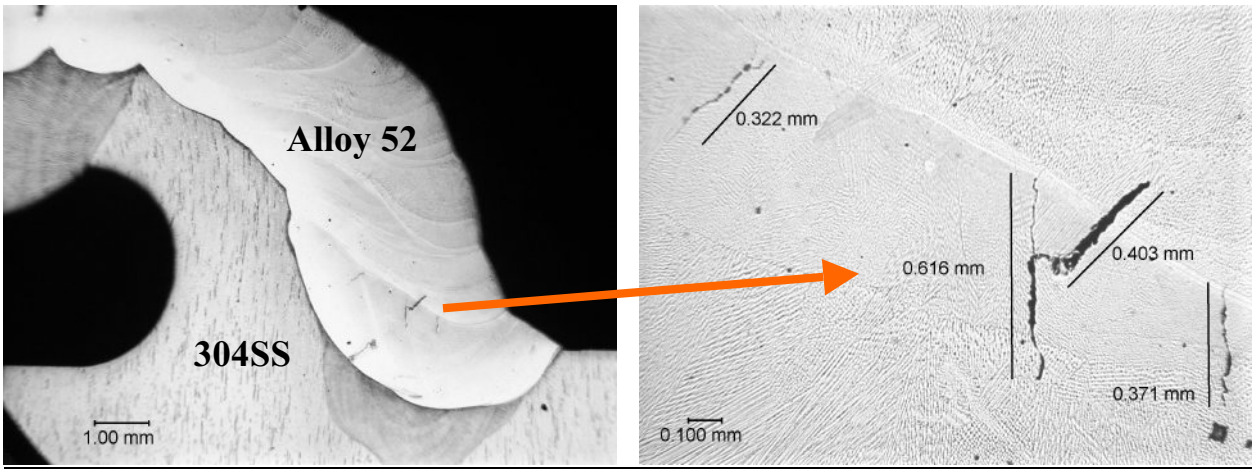

Figure 12. Optical micrographs provided by Ringhals showing the alloy 52 weld metal overlay on a 304SS housing along typical locations of hot cracks.

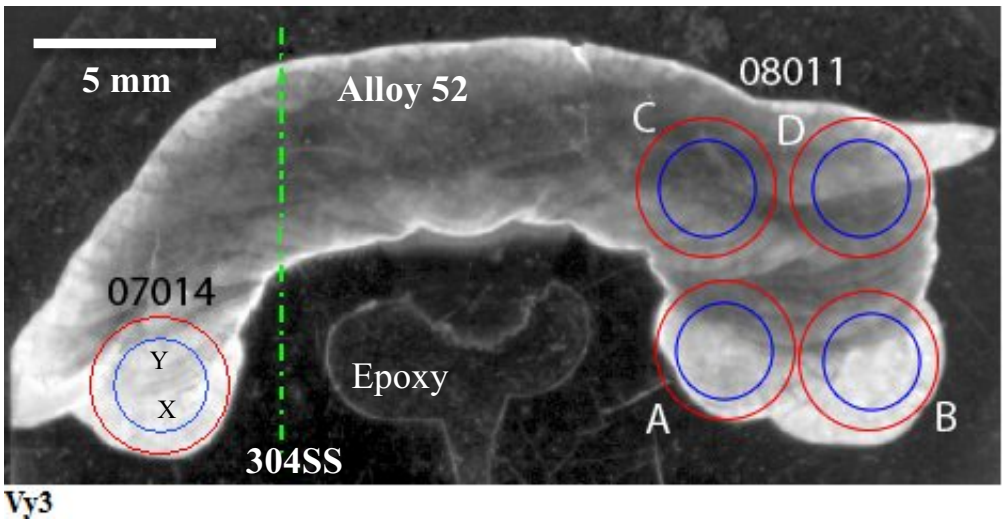

Figure 13. Optical image providing overview of the Ringhals weld overlay sample VY3 after light etching and identifying various regions where TEM samples were prepared.

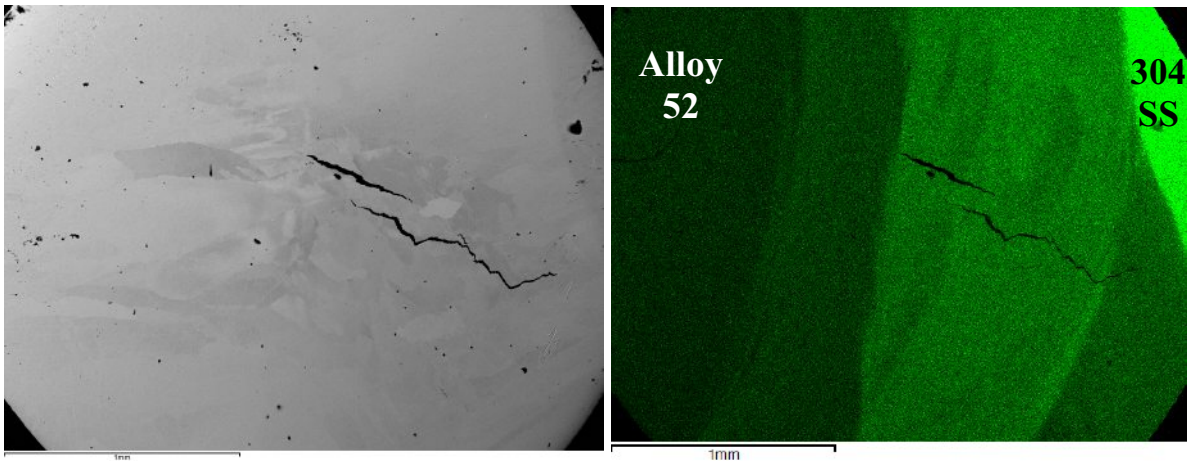

Figure 14. SEM (left) and EDS compositional map for Fe (right) illustrating location of hot cracks in the dilution layer between alloy 52 and 304SS for overlay sample VY3.

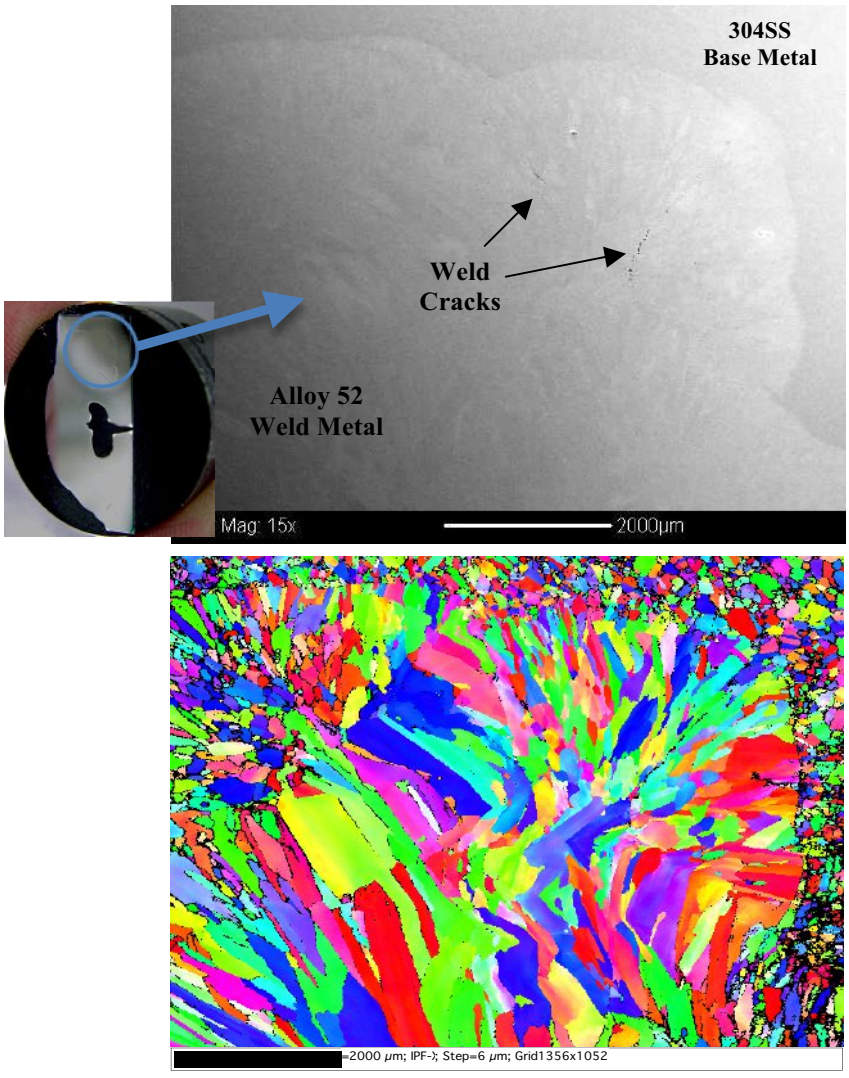

Figure 15. SEM (top) and EBSD IPF-X images (bottom) illustrating the microstructure across the 304SS base metal and weld metal interface region in overlay sample VY4.

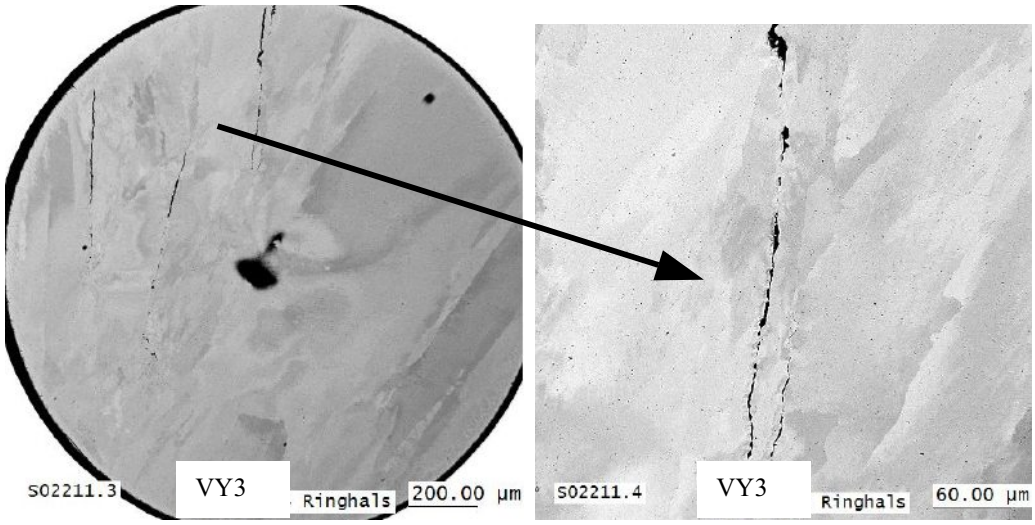

Figure 16. Backscatter SEM images showing weld cracks in alloy 52 overlay sample VY3 and identifying region for ATEM examinations.

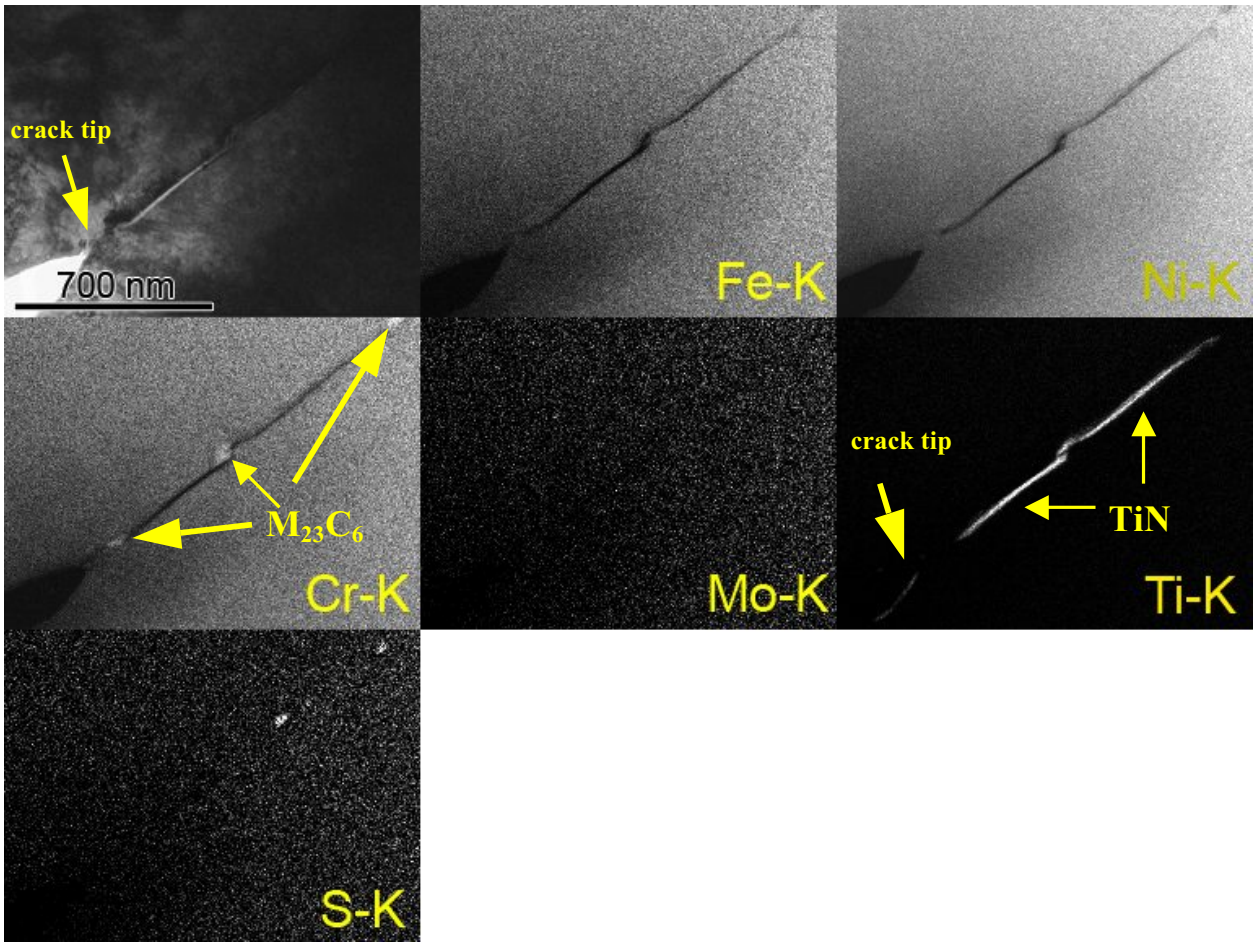

Figure 17. TEM micrograph and elemental maps of an IG crack in alloy 52 overlay sample VY3. A continuous TiN phase is observed along the grain boundary in front of the crack.

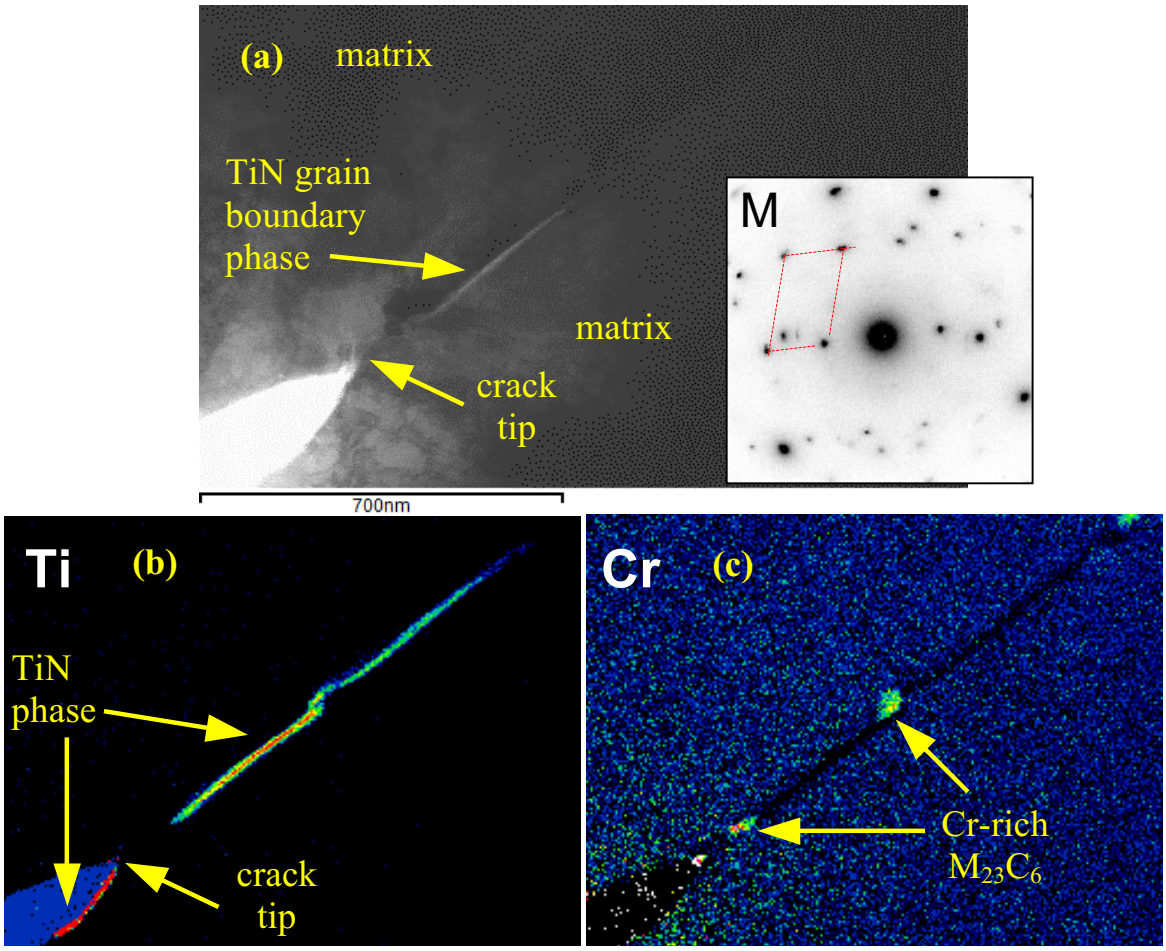

Figure 18. Higher magnification examination of the crack-tip region shown in Figure 17: (a) TEM brightfield image and selected area diffraction identifying a thin MC-structure second phase; (b) EDS map for Ti demonstrating that the thin phase is highly Ti rich and is located on one side of the crack wall and elongated along the grain boundary; and (c) EDS map for Cr highlighting several IG Cr-rich carbides.